Autoignition of *n*-decane droplets in the low-, intermediate-, and high-temperature regimes from a mixture fraction viewpoint

G. Borghesi[1*] and E. Mastorakos[2]

[1]Department of Civil and Mechanical Engineering

California Institute of Technology, Pasadena, CA 91125, USA

[2]Department of Engineering

University of Cambridge, CB2 1PZ Cambridge, UK

Abstract

Detailed numerical simulations of isolated *n*-decane droplets autoignition are presented for different values of the ambient pressure and temperature. The ignition modes considered included single-stage ignition, two-stage ignition and cool-flame ignition. The analysis was conducted from a mixture fraction perspective. Two characteristic chemical time scales were identified for two-stage ignition: one for cool-flame ignition, and another for hot-flame ignition. The appearance and subsequent spatial propagation of a cool flame at lean compositions was found to play an important role in the ignition process, since it created the conditions for activating the high-temperature reactions pathway in regions with locally rich composition. Single-stage ignition was characterized by a single chemical time scale, corresponding to hot-flame ignition. Low-temperature reactions were negligible for this case, and spatial diffusion of heat and chemical species mainly affected the duration of the ignition transient, but not the location in mixture fraction space at which ignition first occurs. Finally, ignition of several cool flames of decreasing strength was observed in the cool-flame ignition case, which eventually lead to a plateau in the maximum gas-phase temperature. The first cool flame ignited in a region where the fuel / air mixture was locally lean, whereas ignition of the remaining cool flames occurred at rich mixture compositions.

1 Introduction

The ignition and subsequent burning of liquid droplets has received considerable attention over the last decades because of its fundamental nature and the insights it provides on spray combustion [1]. Numerical and experimental studies exist for a wide range of fuels, including ethanol [2], methanol [3, 4, 5] and methyl butanoate [6]. Because of their relevance to diesel engines and gas turbine engines combustion, special attention has been reserved to *n*-heptane and *n*-decane. An interesting aspect of these fuels is the variety of ignition modes they display; depending on the

*Corresponding author. Present address: Sandia National Laboratories, Livermore, CA 94550, USA. Email: gborghe@sandia.gov

initial values of pressure and ambient gas temperature considered, four different situations are observed, corresponding to single-stage ignition, two-stage ignition, cool-flame ignition and no ignition [7, 8].

The appearance of cool flames during the combustion of *n*-alkanes liquid droplet was first observed experimentally by Tanabe et al. [7]. Since the publication of this pioneering work, several groups have tried to replicate these findings by means of numerical simulations [8, 9, 10, 11, 12]. Among these studies, the recent work of Cuoci et al. [11] deserves a special mention as the authors were able to reproduce accurately the ignition diagrams (e.g. a diagram showing the ignition mode corresponding to given values of pressure and initial ambient gas temperature) of *n*-heptane, *n*-decane and *n*-dodecane; additionally, for *n*-heptane, ignition delay times were also predicted with good accuracy for a wide range of ambient pressures and temperatures. Despite their high-fidelity, one of the limits of existing numerical works on droplet autoignition is perhaps their excessive focus on chemical kinetics effects. In general, the existence of low- and high-temperature reactions pathways in the oxidation of *n*-alkanes has been identified as the leading cause for the shift between two- and single-stage ignition as the initial ambient gas temperature is increased [8, 10, 11]. Despite chemical kinetics is likely to play a major role in the transition between the different ignition modes, the role of convection and species and heat diffusion is worth a more careful investigation.

Several studies on single- [13, 14] and two-phase [15, 16, 17] turbulent flow autoignition have revealed how ignition first occurs at those locations where scalar fluctuations are low and the mixture has an optimal composition, which depends on pressure and the initial temperatures of the oxidizer and fuel streams. In the specific context of *n*-heptane droplets, Borghesi and Mastorakos [12] have shown that, within the two-stage ignition regime, high-temperature ignition occurs at mixture-rich compositions, and is triggered by the spatial propagation of a cool flame which originates at lean conditions. These results suggest that, under certain conditions, spatial transport may play an important role in the overall ignition process of a droplet and should be investigated in more details.

This paper studies the autoignition of *n*-decane droplets for initial ambient air temperatures below $T_{g,0} < 1000\,\mathrm{K}$ and for pressures between $p = 1$ and 10 bar. These conditions were chosen to allow for the comparison of our results with the large amount of experimental [7, 18] and numerical [10, 11] data that are available in the open literature. The scope of this work is to extend the analysis of *n*-heptane droplet autoignition from a mixture-fraction perspective presented in [12] to *n*-decane, which is a much less volatile fuel. Similarly to what has been done in [12], we will investigate the interactions between chemical reactions and species / heat diffusion that occur during *n*-decane droplet autoignition at low-, intermediate- and high-temperature conditions, with the ultimate aim of providing a deeper understanding of the ignition behaviour of turbulent sprays, the study of which very often revolves around models based on the mixture fraction concept.

2 Mathematical formulation

2.1 Governing equations

Species diffusion and internal motion within the droplet are neglected. Under these assumptions, the set of conservation equations that describe the liquid-phase evolution consists of the mass conservation equation:

$$\overline{\rho}_l \frac{dR_d}{dt} + \frac{R_d}{3}\frac{d\overline{\rho}_l}{dt} = -\rho_g \left(u_g - \frac{dR_d}{dt} \right) = -W_{\text{tot}} \tag{1}$$

and the energy conservation equation:

$$\rho_l C_l \frac{\partial T_l}{\partial t} = \frac{1}{r^2}\frac{\partial}{\partial r}\left(r^2 k_l \frac{\partial T_l}{\partial r} \right) \tag{2}$$

The quantities $\overline{\rho}_l$ and $d\overline{\rho}_l \,/\, dt$ are the volume-averaged liquid-phase density and its temporal derivative. The liquid density and the liquid thermal conductivity were estimated according to Daubert et al. [19] and Latini et al. [19] respectively, while the method of Růžička and Domalski [19] was used for computing the liquid heat capacity.

In the absence of radiative heat transfer, the set of conservation equations that describe the evolution of the gas-phase properties consists of the mass conservation equation:

$$\frac{\partial \rho_g}{\partial t} + \frac{1}{r^2}\frac{\partial}{\partial r}\left(r^2 \rho_g u_g \right) = 0 \tag{3}$$

and the energy equation:

$$\begin{aligned} \rho_g C_{p,g} \left(\frac{\partial T_g}{\partial t} + u_g \frac{\partial T_g}{\partial r} \right) = &-\rho_g \sum_{\alpha=1}^{N-1} \left[C_{p,g,\alpha} \left(Y_{g,\alpha} V_{g,\alpha} - Y_{g,\mathrm{N_2}} V_{g,\mathrm{N_2}} \right) \right] \frac{\partial T_g}{\partial r} \\ &+ \frac{1}{r^2}\frac{\partial}{\partial r}\left[r^2 \kappa \frac{\partial T_g}{\partial r} \right] - \sum_{\alpha=1}^{N} \left(\dot{\omega}_{g,\alpha} h_{g,\alpha} \right) \end{aligned} \tag{4}$$

These equations are supplemented by $N-1$ transport equations for the mass fractions of the chemical species:

$$\begin{aligned} \rho_g \left(\frac{\partial Y_{g,\alpha}}{\partial t} + u_g \frac{\partial Y_{g,\alpha}}{\partial r} \right) = &-\frac{1}{r^2}\frac{\partial}{\partial r}\left(r^2 \rho_g Y_{g,\alpha} V_{g,\alpha} \right) \\ &+ \dot{\omega}_{g,\alpha}, \qquad \alpha = 1, \ldots, N-1 \end{aligned} \tag{5}$$

The N-th species mass fraction is computed from the algebraic constraint $\sum_{\alpha=1}^{N} Y_\alpha = 1$. The gas-phase density was computed with the ideal-gas equation of state. The `TRANSPORT` package [20] is used to evaluate mixture and individual species properties. Species diffusion velocities are computed using a mixture-averaged formulation [20]:

$$V_{g,\alpha} = -\frac{1}{X_\alpha}\mathbb{D}_{\alpha m}\frac{\partial X_\alpha}{\partial r} + V_c, \quad V_c = \sum_{\beta=1}^{N} \frac{Y_\beta}{X_\beta}\mathbb{D}_{\beta m}\frac{\partial X_\beta}{\partial r}.$$

where the mixture-averaged diffusion coefficient $\mathbb{D}_{\alpha m}$ is given by:

$$\mathbb{D}_{\alpha m} = \frac{1 - Y_\alpha}{\sum_{\beta \neq \alpha}^{N} \frac{X_\beta}{D_{\beta\alpha}}}$$

with $D_{\beta\alpha}$ being the binary diffusion coefficients. In the above equations, V_c is a correction to the diffusion velocities; its role is to enforce the constraint $\sum_{\alpha=1}^{N} Y_\alpha V_{g,\alpha} = 0$.

2.2 Interface and boundary conditions

The boundary conditions at the droplet center and in the gas-phase far field can be expressed as:

$$\begin{aligned} r = 0: \quad & \frac{\partial T_l}{\partial r} = 0; \\ r = r_{\max}: \quad & T_g = T_g^0, \quad Y_{g,\alpha} = Y_{g,\alpha}^0, \qquad \alpha = 1, \ldots, N-1 \end{aligned}$$

The first condition is a consequence of the assumption of spherical symmetry. The second condition states that, at sufficiently large distances from the droplet surface, the mixture composition and temperature approach those of the ambient gas.

Phase-equilibrium at the gas-liquid interface requires the equality of both temperature and fugacities of the two phases at the interface:

$$\begin{aligned} r = R_d: \quad & T_l|_{R_d^-} = T_g|_{R_d^+}; \\ & f_{l,\alpha} = f_{g,\alpha}, \quad \alpha = 1, N. \end{aligned}$$

Additionally, conservation of mass and energy across the interface implies that:

$$\begin{aligned} r = R_d: \quad & \kappa_l \left.\frac{\partial T_l}{\partial r}\right|_{R_d^-} + W_{\text{tot}} \Delta H_v = \kappa \left.\frac{\partial T_g}{\partial r}\right|_{R_d^+}; \\ & W_{\text{tot}} \delta_{\alpha F} = W_{\text{tot}} Y_{g,\alpha} + \rho_g Y_{g,\alpha} V_{g,\alpha}, \quad \alpha = 1, N. \end{aligned}$$

with δ being the Kronecker delta. In writing the above equations, we made use of the fact that, in our model, chemical species are not allowed to diffuse into the liquid-phase. Values for the enthalpy of vaporization and the vapor pressure were taken from [19].

2.3 Chemical mechanism

A general, semi-detailed scheme [21] for the pyrolysis, partial oxidation and combustion of heavy n-alkanes was selected. This mechanism consists of 276 species and 8439 reactions; it can be used to simulate the ignition of n-alkanes up to C_{20}, thus including the fuels considered in this work. The mechanism includes both the high- and the low-temperature reactions pathways, and is thus able to capture ignition occurring in the whole range of initial ambient gas temperatures considered. The main reason for choosing the present kinetic model lies in its ability of reproducing the ignition diagrams and accurately predicting the ignition delay times of n-heptane liquid fuel droplets, as it has been recently demonstrated in [11].

2.4 Numerical method and simulations details

The simulation domain extends from $r_{\min} = 0$ to $r_{\max} = 50 d_0$, with d_0 being the initial droplet diameter. The governing equations were discretized using the Method of Lines. Second-order central difference stencils were used

for the diffusive terms, whereas convective terms were treated using a first-order upwind scheme. The numerical grids for the liquid and gaseous phases consist of 40 and 240 nodes respectively. The nodes in the gaseous-phase are clustered in the surrounding of the gas-liquid interface using the rule $\Delta r_{i+1} = 1.03 \cdot \Delta r_i$, with Δr_i being the distance between nodes i and $i+1$. Equidistant nodes were used for the discretization of the liquid phase. The solution of the resulting system of Differential-Algebraic Equations (DAE) was computed with the implicit solver DASPK [22]. DASPK requires the evaluation of the Jacobian matrix of the system to perform an integration step. To minimize the computational time, the Jacobian was evaluated analytically and care was taken in writing the system in block-diagonal form. Terms that did not maintain the banded structure of the Jacobian matrix were treated as additional unknowns using dummy algebraic equations, as explained in [23]

Unless otherwise specified, the initial droplet diameter was $d_0 = 0.7\,\mathrm{mm}$ for all simulated cases. The liquid temperature T_l was initialized by assuming a linear variation between $T_{l,0} = 300\,\mathrm{K}$ for $T_{g,0} = 600\,\mathrm{K}$ and $T_{l,0} = 320\,\mathrm{K}$ for $T_{g,0} = 1000\,\mathrm{K}$. This initialization procedure is identical to the one followed in [8] for n-heptane droplets.

2.5 Post-processing of simulation data

In processing the numerical results, a mixture fraction ξ based on elemental mass fraction was used [24]. For a generic fuel species $C_m H_n$, ξ is computed as:

$$
\begin{aligned}
&\xi = \frac{\beta - \beta_0}{\beta_F - \beta O};\\
&\beta = \sum_{\alpha=1}^{N} \left\{ \gamma_C W_C a_{C,\alpha} + \gamma_H W_H a_{H,\alpha} + \gamma_O W_O a_{O,\alpha} \right\} \frac{Y_\alpha}{W_\alpha};\\
&\gamma_C = \frac{1}{m W_C}, \qquad \gamma_H = \frac{1}{n W_H}, \qquad \gamma_O = -\frac{1}{(m + n/4)\, W_O}.
\end{aligned}
$$

where $a_{l,\alpha}$ denotes the number of atoms of element l in species α. In the above equation, β_0 and β_F are the values of β in the oxidizer and fuel streams respectively.

As this work deals with single- and two-stage ignition of liquid droplets, criteria for identifying the occurrence of an ignition event must be established. Following Schnaubelt et al. [8], cool-flame ignition was detected according to the following criterion:

$$
\frac{\partial T_{\max}(t)}{\partial t} \geq 10^4\,\mathrm{K/s}
$$

where $T_{\max}$ is the maximum gas-phase temperature. The hot-flame ignition criterion, on the other hand, was $T_{\max} > 1350\,\mathrm{K}$. Criteria based on the derivative of the gas-phase temperature with respect to time were also tested for completeness, and they yielded similar results.

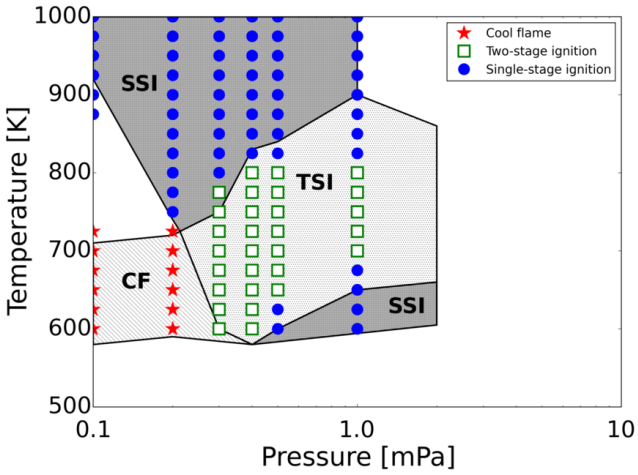

Figure 1: Ignition diagram of *n*-decane in air for different values of the ambient pressure. Filled regions correspond to the experimental data of Moriue et al. [18], while each symbol is representative of a numerical simulation. CF indicates cool flames, TSI two-stage ignition and SSI single-stage ignition.

3 Results

3.1 Validation of computational code and description of ignition modes

The ignition modes of quiescent *n*-decane droplets in air are shown in Figure 1 for different values of pressure and initial ambient gas temperature. Good agreement is found between numerical simulations and the experimental data of Moriue et al. [18], thus indicating that the mathematical model for single-droplet combustion presented in this work is able to capture most aspects of the physics of *n*-decane droplet autoignition. The results shown in Figure 1 are also very similar to those obtained by Cuoci et al. [11]; this is not surprising since the chemical mechanism used in that work is an updated version of the one adopted here. This similarity provides a further validation of the numerical code used for the simulations presented in this study. Additional validation of our code is provided in [12], and the interested reader is referred there for further details.

The temporal evolution of the maximum gas-phase temperature $T_{g,\max}$ is shown in Figure 2 for selected values of pressure and initial gas-phase temperature, corresponding to single-stage ignition **(a)**, two-stage ignition (**(b)** and **(c)**) and cool flame ignition **(d)**. All cases investigated include an initial period of time during which $T_{g,\max} = T_{g,0}$ and the amount of heat released by chemical reactions is negligible. This phase is characterized by the heating and evaporation of the liquid droplet and by the mixing of the resulting fuel vapor with the ambient gas to yield an ignitable mixture. Once conditions favorable to mixture ignition have been created, the subsequent evolution of the system depends on the ignition mode considered. Single-stage ignition is characterized by a rapid, monotonic increase in $T_{g,\max}$, which reaches the value corresponding to a burning diffusion flame shortly after $T_{g,\max}$ becomes larger than $T_{g,0}$. This ignition mode is usually associated with the high-temperature reactions pathway of *n*-alkanes. Two-stage ignition, as its name suggests, occurs in two separate phases; first, an increase in $T_{g,\max}$ above $T_{g,0}$ is

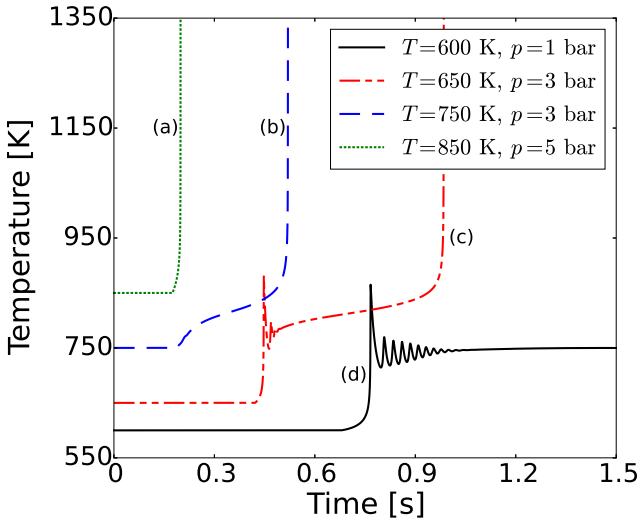

Figure 2: Temporal evolution of maximum gas-phase temperature for selected values of pressure and initial ambient gas temperature. The initial droplet diameter was $d_0 = 0.7\,\mathrm{mm}$ for all simulated cases.

observed, then an induction period characterized by a slow growth in $T_{g,\max}$ follows, and finally thermal runaway occurs. Depending on the initial value of the ambient gas temperature, the initial increase in $T_{g,\max}$ may occur more or less suddenly, as shown by curves **(b)** and **(c)** in Figure 2. Two-stage ignition is a consequence of the existence of a low-temperature reactions pathway for *n*-alkanes on top of the high-temperature one; in fact, the initial slow increase in $T_{g,\max}$ observed in two-stage ignition, which plays a major role in creating the conditions for high-temperature reactions to become significant at the end of the induction time, is due to low-temperature reactions [8, 10, 11]. Finally, cool flame ignition is characterized by an increase in $T_{g,\max}$ over $T_{g,0}$ of up to 200 K, depending on the initial values of pressure and ambient gas temperature considered. As shown by curve **(d)** in Figure 2, the transition is not necessarily monotonic, but may occur under the form of several oscillating cool flames, whose amplitude is progressively damped until a plateau in the value of $T_{g,\max}$ is reached. In this case, low-temperature reactions are responsible for the increase in $T_{g,\max}$ over $T_{g,0}$: this increase in temperature, however, is not sufficient to trigger the high-temperature reactions pathway.

3.2 Two-stage, low-temperature autoignition

We start our analysis by investigating the physics of two-stage, low temperature *n*-decane droplet autoignition. To this scope, we plotted in Figure 3 the ξ-profiles of temperature and selected species mass fractions at different instants of time prior, during and after ignition. The data shown correspond to $p = 3\,\mathrm{bar}$ and $T_{g,0} = 650\,\mathrm{K}$: these conditions are associated with two-stage ignition. Early during the ignition transient (e.g. when $t < 0.2\,\mathrm{s}$), the amount of heat released by chemical reactions is negligible and the profile of T_g versus ξ corresponds to frozen mixing between the fuel vapor and the ambient gas. At later times, exothermic reactions become important and an increase in

the ambient gas temperature with respect to the frozen mixing line[1] can be observed. When the increase in T_g is sufficiently large, a cool flame ignites in the lean mixture region around $\xi = 0.03$ (for n-decane in air, $\xi_{\rm st} = 0.06265$) at $t \simeq 0.445\,{\rm s}$ and then rapidly propagates in mixture fraction space, leading to a considerable rise in the gas-phase temperature over a large interval of ξ values. Additionally, once cool-flame ignition occurs, the liquid droplet experiences strong heating, as revealed by the rapid increase in the value of the maximum mixture fraction, which is directly proportional to the liquid saturation pressure. The cool-flame propagation phase can also be observed from the temporal evolution of the mass fraction of the n-decane ketohydroperoxides, $Y_{n\text{-}{\rm C_{10}}\text{-}{\rm OQOOH}}$, which are precursor species for low-temperature ignition [8, 10, 11]. The ξ-profiles of $Y_{n\text{-}{\rm C_{10}}\text{-}{\rm OQOOH}}$ are shown in Figure 3b; these curves reveal the early build-up of this important species, followed by its rapid consumption as the cool flame is ignited and starts propagating towards the neighbouring regions. Once the cool flame has established itself over the entire range of ξ values, the ambient-gas temperature at any mixture composition has become high enough to activate the high-temperature reactions pathways and an hot ignition kernel starts developing around $\xi = 0.3$, where the mixture is locally rich. The location of maximum gas-phase temperature slowly shifts with time towards $\xi = 0.2$; ignition occurs at this latter mixture fraction location when $t \simeq 0.985\,{\rm s}$. Following ignition, two reaction fronts are seen to propagate rapidly towards leaner and richer mixtures, leading to the formation of a diffusion flame shortly after. The reaction zone dynamics just discussed is confirmed by the temporal evolution of the ξ-profiles of OH and CO_2, which are shown in Figures 3c and 3d respectively. The hot-flame ignition sequence described here is similar in many aspects to the ignition of the unsteady fuel / air mixing layer problem studied by Linãn and Crespo [25]. From the above discussion, it is clear that two-stage ignition is characterized by two characteristics chemical time scales: a time scale for cool-flame ignition, and a time scale for hot flame ignition. The relevant chemical processes associated with these time scales occur at different mixture compositions: more specifically, the cool flame ignites where ξ is locally lean, whereas the opposite is true for the hot flame. A direct consequence of this complex behavior is the difficulty in predicting accurately the location of the ignition spot in mixture fraction space from homogeneous reactor calculations. As suggested by Mastorakos [14], the computation of the ignition delay time of homogeneous air / fuel mixtures is an useful tool in that it provides estimate of where autoignition will occur in mixture fraction space, and can also identify the order of magnitude of the actual autoignition time. These calculations, however, cannot account for spatial diffusion of heat and chemical species; as such, they may not be very significative for two-stage ignition, where these effects play a key role in the hot-flame ignition process.

3.3 Single-stage, high-temperature autoignition

The role played by low-temperature reactions in the ignition process becomes less important and eventually disappear as the value of the initial ambient temperature is increased. One would then expect hot-flame ignition to occur around a single mixture fraction location, without the prior propagation of a cool flame in mixture fraction space. To verify this point, we plotted in Figure 4 the ξ-profiles of temperature and selected species mass fractions for a single-stage

[1]The frozen mixing line is the straight line connecting $T_g(\xi = 0)$ with $T_g(\xi = \xi_{\rm max}(t))$, where $\xi_{\rm max}(t)$ is the maximum value of the mixture fraction, which occurs at the droplet surface.

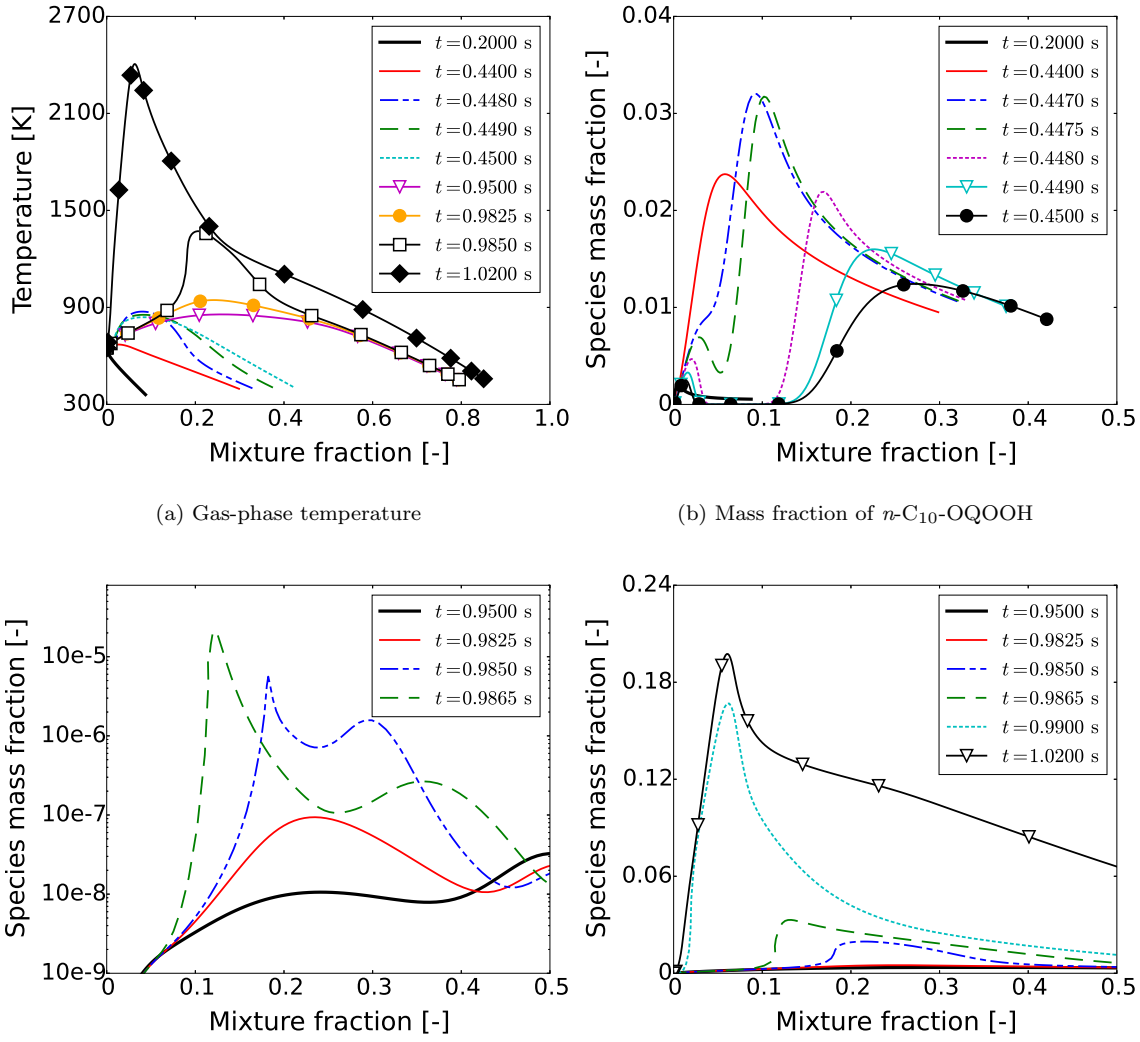

(a) Gas-phase temperature

(b) Mass fraction of n-C_{10}-OQOOH

(c) Mass fraction of OH

(d) Mass fraction of CO_2

Figure 3: Gas-phase temperature and selected species mass fractions plotted against mixture fraction at selected instants of time. Data shown correspond to $p = 3\,\text{bar}$ and $T_{g,0} = 650\,\text{K}$.

ignition case, corresponding to $T_{g,0} = 950\,\text{K}$ and $p = 5\,\text{bar}$. Similarly to the approach followed for the low-temperature ignition case, the profiles have been plotted at selected instants of time during the ignition transient. It is seen from Figure 4a that an ignition kernel develops at early times around $\xi = 0.019$, leading to a rapid increase in the local gas-phase temperature. Some of the heat generated at the location of first kernel appearance is conducted towards the neighbouring spatial regions, resulting in a speed-up of the local chemical reactions. No reaction wave is seen to propagate in mixture fraction space during this phase. This latter point is also confirmed by the low values of the n-decane ketohydroperoxides mass fraction throughout the entire ignition transient, especially in the region where the ignition kernel develops, as shown by Figure 4b. Once the flame ignites, two premixed flames are seen to propagate towards leaner and richer mixture compositions; this is particularly evident from the temporal evolution

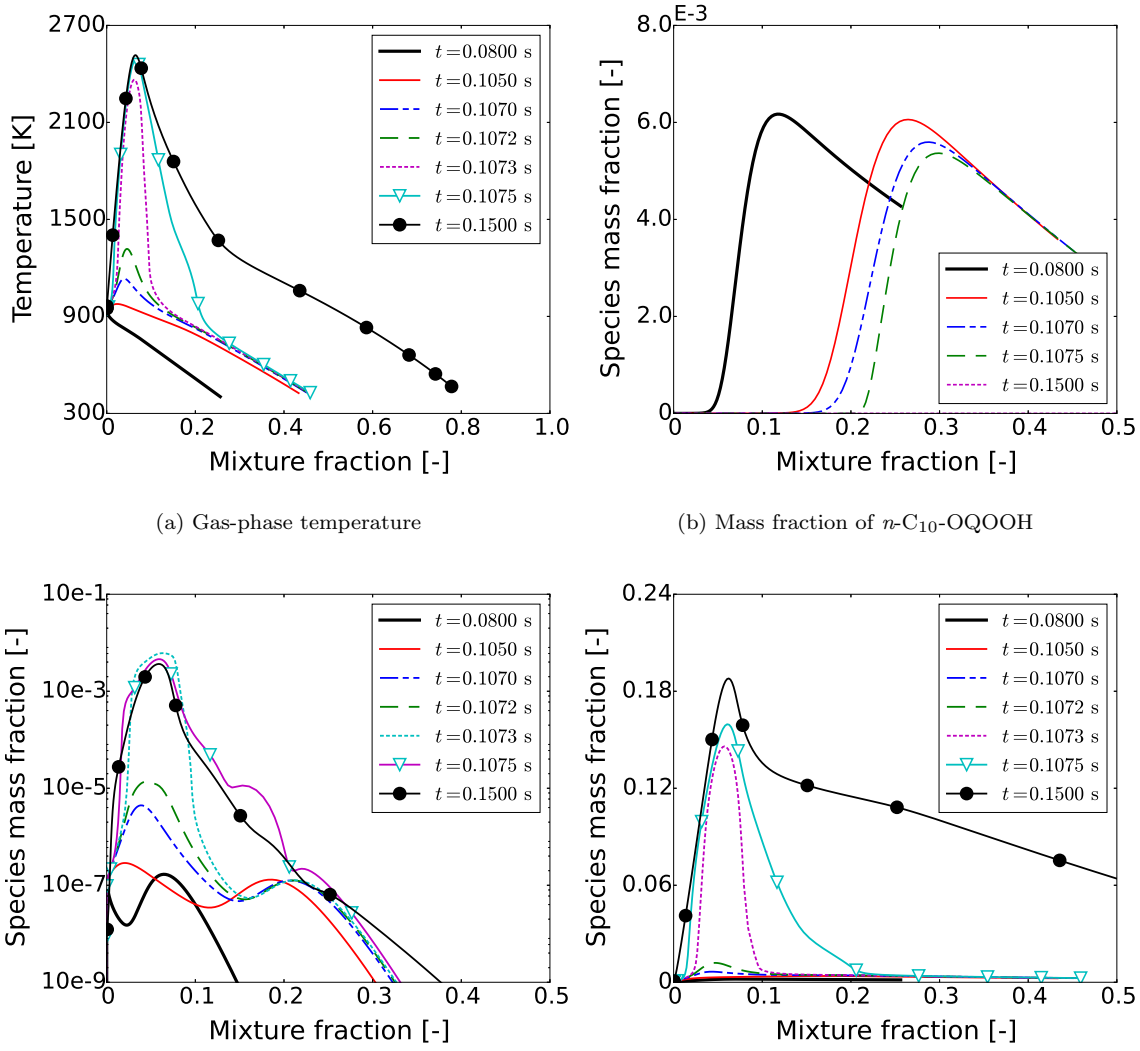

(a) Gas-phase temperature

(b) Mass fraction of n-C_{10}-OQOOH

(c) Mass fraction of OH

(d) Mass fraction of CO_2

Figure 4: Gas-phase temperature and selected species mass fractions plotted against mixture fraction at selected instants of time. Data shown correspond to $p = 5\,\mathrm{bar}$ and $T_{g,0} = 950\,\mathrm{K}$.

of the ξ-profiles of Y_{OH} and $Y_{\mathrm{CO_2}}$, which are shown in Figures 4c and 4d respectively. At the end of the ignition transient, a diffusion flame is established around the droplet. It is clear that, differently from the low-temperature case, high-temperature ignition is characterized by a single chemical time scale, and also by a single location in mixture fraction space where the transition from a frozen solution to a burning flame first occurs. Spatial diffusion of heat and chemical species may still affect the ignition process, most notably by subtracting heat and reactive radicals from the ignition kernel; however, the role played by these processes is considerably less important than the corresponding one in two-stage ignition. Due to this simpler behaviour, it is expected that homogeneous reactor calculations should be able to capture with good accuracy the location of the ignition spot in mixture fraction space.

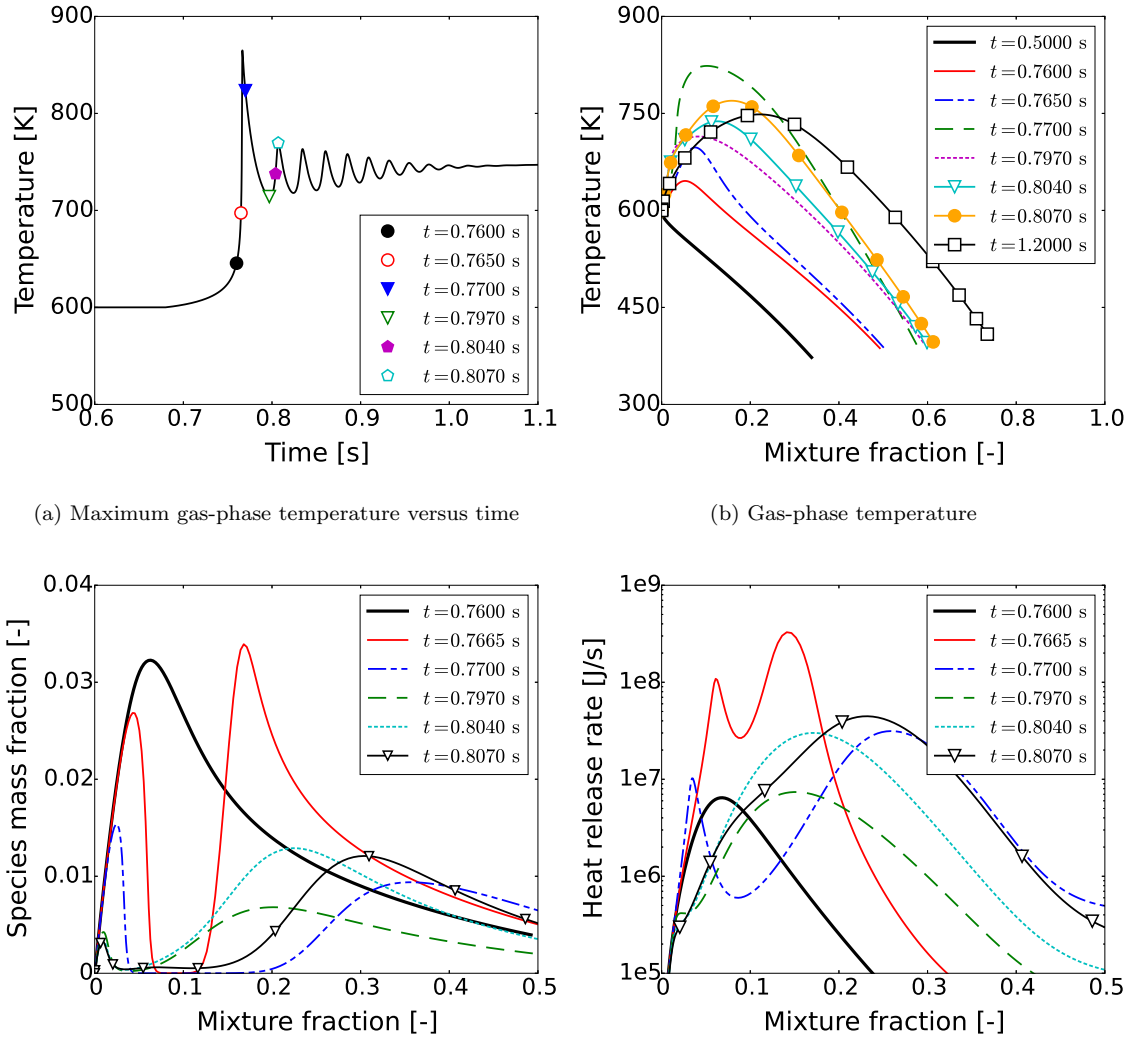

(a) Maximum gas-phase temperature versus time

(b) Gas-phase temperature

(c) Mass fraction of n-C_{10}-OQOOH

(d) Heat release rate

Figure 5: Top-left figure: temporal evolution of maximum gas-phase temperature versus time. Remaining figures: profiles of gas-phase temperature, heat release rate and n-C_{10}-OQOOH mass fraction plotted against mixture fraction at selected instants of time. Data shown correspond to $p = 1\,\text{bar}$ and $T_{g,0} = 600\,\text{K}$.

3.4 Cool-flame autoignition

To conclude the analysis of the phenomena occurring during the different ignition modes of n-decane droplets, we provide a detailed discussion of the case with initial conditions given by $T_{g,0} = 600\,\text{K}$ and $p = 1\,\text{bar}$, which corresponds to cool-flame ignition. The mixture fraction profiles of gas-phase temperature, heat release rate and mass fraction of n-C_{10}-OQOOH for this case are shown in Figure 5 at selected instants of time during the ignition transient. For the sake of clarity, these time stations have been marked in Figure 5a, which shows the temporal evolution of the maximum value of the gas-phase temperature. Similarly to the situation observed in the low-temperature ignition case, an increase in T_g above the frozen mixing line is first observed in correspondence of lean values of

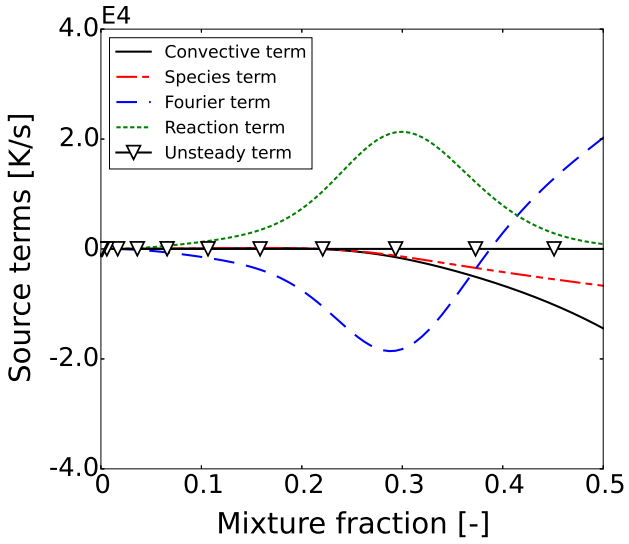

Figure 6: Source terms appearing in the gas-phase energy equation. Data shown at $t = 1.2\,\mathrm{s}$ for $T_{g,0} = 600\,\mathrm{K}$ and $p = 1\,\mathrm{bar}$.

ξ, followed by ignition and subsequent propagation of a cool flame in mixture fraction space. During this phase, the *n*-decane ketohydroperoxides are consumed quickly, as shown in Figure 5c, leading to a decrease in the amount of heat released in these regions; as a consequence, the gas-phase temperature, after reaching a peak value, starts to decrease rapidly since heat diffusion is no longer balanced by exothermic reactions. This decrease in temperature generates conditions that are favorable to a secondary growth of ketohydroperoxides, which now occurs around $\xi = 0.2$; at these mixture compositions, the mass fractions of these intermediate species is seen to increase until a critical concentration is reached, after which ignition and propagation of a secondary cool flame is observed. The peak in temperature associated with the secondary cool flame is lower than that of the main one due to the smaller amount of ketohydroperoxides formed between the two cool flames ignition events. Further peaks of decreasing amplitude in the temporal trace of $T_{g,\max}$ are observed after ignition of the secondary cool flame, until a plateau is eventually reached; these oscillations can be explained again as the consequence of rapid depletion and formation of ketohydroperoxides at rich mixture compositions, which result in subsequent ignitions and spatial propagations of progressively weaker cool flames. The mechanism for cool flame oscillations described here is somewhat similar the one observed in homogeneous mixtures [26], where a phase relationship between temperature and concentration of a peroxydic, molecular branching intermediate is observed.

The cool-flame ignition case does not result in hot flame ignition after the cool flame appearance, differently from what observed for the low-temperature ignition case. To better understand this point, we plotted in Figure 6 the budget of terms appearing in the gas-phase energy equation at $t = 1.2\,\mathrm{s}$. For the sake of the present analysis, five different contributions (including the unsteady term) to the energy balance were identified from Equation 4:

$$\Pi_1 = -\rho C_{p,g} u_g \frac{\partial T_g}{\partial r}, \quad \Pi_2 = \frac{\partial T}{\partial t}, \quad \Pi_3 = \frac{1}{r^2}\frac{\partial}{\partial r}\left[r^2 \kappa \frac{\partial T_g}{\partial r}\right],$$
$$\Pi_4 = \rho_g \sum_{\alpha=1}^{N-1} \left[C_{p,g,\alpha}\left(Y_{g,\alpha} V_{g,\alpha} - Y_{g,\mathrm{N_2}} V_{g,\mathrm{N_2}}\right)\right] \frac{\partial T_g}{\partial r}, \quad \Pi_5 = -\sum_{\alpha=1}^{N} \left(\dot{\omega}_{g,\alpha} h_{g,\alpha}\right).$$

which correspond to convection, the unsteady term, Fourier heat diffusion, species heat diffusion and chemical reactions. The dominant contributions to the balance of terms are due to chemical reactions and Fourier heat diffusion, which approximately balance each other. Convection and species heat diffusion are negligible, apart for very high values of ξ. In the entire mixture fraction space, the unsteady term, which is given by the sum of the remaining source terms, is approximately zero, thus explaining why $T_{g,\max}$ remains constant and hot-flame ignition does not occur.

4 Conclusions

Ignition in isolated *n*-decane droplets under quiescent conditions was studied by means of detailed numerical simulations. The range of conditions investigated was chosen to obtain single-stage ignition, two-stage ignition and cool-flame ignition. A detailed investigation of the droplet ignition phase was conducted for three selected cases representative of these ignition modes. This work extends our previous analysis of *n*-heptane droplet autoignition from a mixture-fraction perspective to *n*-decane, which is a much less volatile fuel. Two-stage ignition, as its name suggests, occurred in two separate phases. The first stage was characterized by the formation of an ignitable mixture and by the appearance of a cool flame in a region where the local mixture composition was very lean and the local temperature was close to the initial ambient temperature. The second stage of ignition started with the quick propagation of the cool flame in mixture fraction space and the subsequent formation of an hot-ignition kernel in the rich side of stoichiometry. The propagation of the cool flame towards rich mixture regions following its ignition was found to play a fundamental role in creating adequate local conditions for the activation of the high-temperature reactions pathway. Due to the fundamental role played by spatial diffusion of heat and species in the ignition process, it was argued that predicting the ignition location in mixture fraction space by means of homogeneous reactor calculations may be difficult.

In the single-stage ignition case, the ignition kernel was observed to develop first in correspondence of lean values of ξ, where the local gas-phase temperature increased monotonically until a burning state was reached. Throughout the entire ignition transient, the maximum value of the *n*-decane ketohydroperoxides mass fraction, which are precursor species for cool-flame ignition, remained low, thus suggesting that the role played by low-temperature reactions for this case is marginal. Differently from the two-stage ignition case, the main effect of spatial diffusion was to remove heat and radicals species from the ignition kernel, thus affecting the ignition delay time, but not the ignition location in mixture fraction space; as a consequence, it was concluded that homogeneous reactor calculations should be able to predict the ξ location of ignition with reasonable accuracy.

Finally, cool-flame ignition, similarly to two-stage ignition, was characterized by the appearance and subsequent propagation of a cool flame in a region where the local mixture composition was very lean. Once formed, the cool flames consumed the *n*-decane ketohydroperoxides and, as a consequence, the maximum gas-phase temperature, after reaching a peak values, started to decrease rapidly since heat-release reactions were no longer present. The decrease in temperature created the conditions for a secondary growth of ketohydroperoxides at rich mixture compositions, which eventually lead to the ignition of a second cool-flame. Further peaks of decreasing amplitude in the temporal trace of the maximum gas-phase temperature were observed after ignition of the secondary cool flame, until a plateau was eventually reached; these oscillations were explained as the consequence of rapid depletion and formation of ketohydroperoxides at rich mixture compositions, which resulted in subsequent ignitions and spatial propagations of progressively weaker cool flames. The plateau was characterized by an almost perfect balance between chemical reactions and Fourier heat diffusion, which inhibited further temperature growth.

5 References

References

[1] S. Aggarwal, "Single droplet ignition: theoretical analyses and experimental findings," *Progress in Energy and Combustion Science*, vol. 45, pp. 79–107, 2014.

[2] A. Kazakov, J. Conley, and F. Dryer, "Detailed modeling of an isolated, ethanol droplet combustion under microgravity conditions," *Combustion and Flame*, vol. 134, pp. 301–314, 2003.

[3] A. Marchese and F. Dryer, "The effect of liquid mass transport on the combustion and extinction of bicomponent droplets of methanol and water," *Combustion and Flame*, vol. 105, pp. 104–122, 1996.

[4] K. Okai, O. Moriue, M. Araki, M. Tsue, M. Kono, J. Sato, D. Dietrich, and F. Williams, "Pressure effects on combustion of methanol and methanol / dodecanol single droplets and droplet pairs in microgravity," *Combustion and Flame*, vol. 121, pp. 501–512, 2000.

[5] R. Stauch and U. Maas, "The ignition of methanol droplets in a laminar convective environment," *Combustion and Flame*, vol. 153, pp. 45–57, 2008.

[6] T. Farouk, Y. Liu, A. Savas, C. Avedisian, and F. Dryer, "Sub-millimeter sized methyl butanoate droplet combustion: microgravity experiments and detailed numerical modeling," *Proceedings of the Combustion Institute*, vol. 34, pp. 1609–1616, 2013.

[7] M. Tanabe, T. Bolik, C. Eigenbrod, H. Rath, J. Sato, and M. Kono, "Spontaneous ignition of liquid droplets from a view of non-homogeneous mixture formation and transient chemical reactions," *Proceedings of the Combustion Institute*, vol. 26, pp. 1637–1643, 1996.

[8] S. Schnaubelt, O. Moriue, T. Coorder, C. Eigenbrod, and H. Rath, "Detailed numerical simulations of the multi-stage self-ignition process of *n*-heptane isolated droplets and their verification by comparison with microgravity experiments," *Proceedings of the Combustion Institute*, vol. 28, pp. 953–960, 2000.

[9] J.-R. Yang and S.-C. Wong, "On the suppression of negative temperature coefficient (NTC) in autoignition of *n*-heptane droplets," *Combustion and Flame*, vol. 132, pp. 475–491, 2003.

[10] A. Cuoci, M. Mehl, G. Buzzi-Ferraris, T. Faravelli, D. Manca, and E. Ranzi, "Autoignition and burning rates of fuel droplets under microgravity," *Combustion and Flame*, vol. 143, pp. 211–226, 2005.

[11] A. Cuoci, A. Frassoldati, T. Faravelli, and E. Ranzi, "Numerical modeling of auto-ignition of isolated fuel droplets in microgravity," *Proceedings of the Combustion Institute*, vol. 35, pp. 1621–1627, 2015.

[12] G. Borghesi and E. Mastorakos, "Spontaneous ignition of isolated n-heptane droplets at low, intermediate, and high ambient temperatures from a mixture-fraction perspective," *Combustion and Flame*, vol. 162, pp. 2544–2560, 2015.

[13] E. Mastorakos, T. Baritaud, and T. Poinsot, "Numerical simulations of autoignition in turbulent mixing flows," *Combustion and Flame*, vol. 109, pp. 198–223, 1997.

[14] E. Mastorakos, "Ignition of turbulent non-premixed flames," *Progress in Energy and Combustion Science*, vol. 35, pp. 57–97, 2009.

[15] P. Schroll, A. Wandel, R. Cant, and E. Mastorakos, "Direct numerical simulations of autoignition in turbulent two-phase flows," *Proceedings of the Combustion Institute*, vol. 32, pp. 2275–2282, 2009.

[16] G. Borghesi, E. Mastorakos, C. Devaud, and R. Bilger, "Modeling evaporation effects in conditional moment closure for spray autoignition," *Combustion Theory and Modelling*, vol. 15, pp. 725–752, 2011.

[17] G. Borghesi, E. Mastorakos, and R. Cant, "Complex chemistry dns of n-heptane spray autoignition at high pressure and intermediate temperature conditions," *Combustion and Flame*, vol. 160, pp. 1254–1275, 2013.

[18] O. Moriue, C. Eigenbrod, H. Rath, J. Sato, K. Okai, M. Tsue, and M. Kono, "Effects of dilution by aromatic hydrocarbons on staged ignition behavior of n-decane droplets," *Proceedings of the Combustion Institute*, vol. 28, pp. 969–975, 2000.

[19] B. Poling, J. Prausnitz, and J. O'Connell, *The properties of gases and liquids.* McGraw-Hill, fifth ed., 2000.

[20] R. Kee, G. Dixon-lewis, J. Warnatz, M. Coltrin, and J. Miller, "A fortran computer code package for the evaluation of gas-phase, multicomponent transport properties," tech. rep., SAND86-8246, 1986.

[21] E. Ranzi, A. Frassoldati, S. Granata, and T. Faravelli, "Wide-range kinetic modeling study of the pyrolysis, partial oxidation and combustion of heavy n-alkanes," *Industrial and Engineering Chemistry Research*, vol. 44, pp. 5170–5183, 2005.

[22] P. Brown, A. Hindmarsh, and L. Petzold, "Using krylov methods in the solution of large-scale differential-algebraic systems," *SIAM Journal on Scientific Computing*, vol. 15, pp. 1467–1488, 1994.

[23] S. Cho, R. Yetter, and F. Dryer, "A computer model for one-dimensional mass and energy transport in and around chemically reacting particles, including gas-phase chemistry, multicomponent molecular diffusion, surface evaporation, and heterogeneous reaction," *Journal of Computational Physics*, vol. 102, pp. 160–179, 1992.

[24] R. Bilger, S. Stårner, and R. Kee, "On reduced mechanisms for methane-air combustion in nonpremixed flames," *Combustion and Flame*, vol. 80, pp. 135–149, 1990.

[25] A. Linan and A. Crespo, "An asymptotic analysis of unsteady diffusion flames for large activation energies," *Combustion Science and Technology*, vol. 14, pp. 95–117, 1976.

[26] R. Fairlie, J. Griffiths, and H. Pearlman, "A numerical study of cool flame development under microgravity," *Proceedings of the Combustion Institute*, vol. 28, pp. 1693–1699, 2000.